

Remote Sensing of Spacecraft Electrostatic Potential Using Secondary Electrons

Miles Bengtson, Joseph Hughes, and Hanspeter Schaub

Abstract—A method is proposed to use secondary electrons to remotely sense the electrostatic potential of an object in geosynchronous orbit or deep space. This method involves a positively charged servicing craft which directs a high energy electron beam at the object of interest such that low energy secondary electrons are emitted from the surface. The low energy electrons emitted by the target are accelerated toward the servicing craft and arrive with an energy equal to the potential difference between the two craft. The servicing craft measures the electron energy spectrum and, knowing its own potential, then infers the potential of the target. Depending on the application, photoelectrons could similarly be used to infer the target potential or the energetic electron beam could be pulsed so that the transferred charge is minimal. Though it is possible to measure potential by directly contacting a surface, remote measurement offers significant advantages and supports missions which must operate in close proximity without making physical contact. Several missions have been proposed that use interactions between charged objects to create useful forces and torques, including electrostatic detumbling and reorbiting of debris, Coulomb formations, and virtual structures. Remote measurement of potential would benefit these missions by enabling feedback control of the active charging. Other applications include mitigation of arcing during rendezvous, docking, and proximity operations for future servicing or salvaging missions. The touchless sensing method can also be applied to map the charge distribution on lunar or asteroid surfaces, helping to characterize the dust electrostatically lofted from the surface.

I. INTRODUCTION

A. Concept

Though spacecraft charging has been studied for decades, there is a lack an understanding of how to effectively sense and monitor the charge on a space object from a distance. Whereas it is possible for a satellite to measure it's own charge using plasma instruments, little research has been done on remotely sensing the charge on another space object. This paper discusses the prospects and challenges of a promising method for remote sensing of the electrostatic potential of a nearby space object. This method involves measuring the energy distributions of electrons which are emitted from the target object. Secondary electrons, generated when an energetic particle impacts a metallic surface, and photoelectrons are both emitted from the conducting surface with almost zero

Miles Bengtson is a graduate research assistant at the University of Colorado Boulder, (email: Miles.Bengtson@colorado.edu)

Joseph Hughes is a graduate research assistant at the University of Colorado Boulder, (email: Joseph.Hughes@colorado.edu)

Hanspeter Schaub is a Professor and Glenn L. Murphy Chair of Engineering at the University of Colorado at Boulder, (email: Hanspeter.Schaub@colorado.edu)

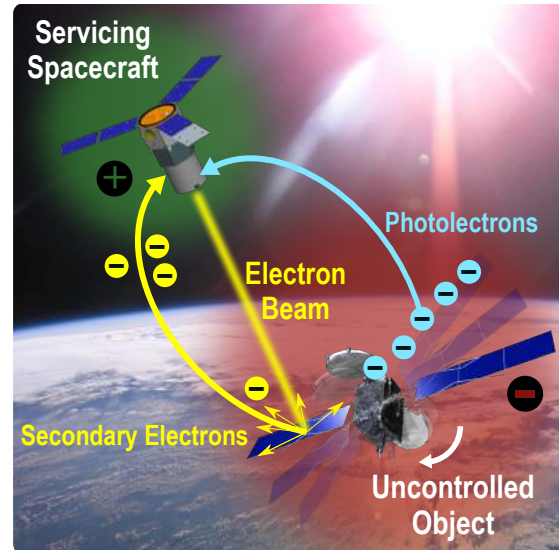


Fig. 1. A servicing craft observes the secondary electrons and photoelectrons emitted by a target object to remote sense the object's electrostatic potential.

energy. A closely co-orbiting servicing satellite that is multiple craft radii apart achieves a high positive potential relative to the target to measure the initially low-energy electrons which are accelerated toward the servicing craft. The electrons arrive with an energy equal to the potential difference between the two craft plus their initial kinetic energy. Therefore, by knowing the potential of the servicing craft, the potential of the target object is inferred. For forced charging applications, the servicing craft directs an electron beam at the target to generate the secondaries. For natural charging, photoelectrons or secondaries generated from ambient plasma currents allow the technique to be used passively. Figure 1 shows a concept of operations for the proposed remote sensing technique.

B. Applications

The ability to remotely sense spacecraft potential has a broad range of applications. As electrical discharges and arcs between differentially charged surfaces can be detrimental to satellite components, remote potential sensing could be used for on-orbit experiments to better understand differential charging and subsequent arcing, thereby allowing electrostatic-related anomalies or mission failures to be mitigated. There is a similar risk of electrostatic discharge for proximity operations and docking with uncharacterized objects which may float at different potentials [1]. Carruth et al. identified that, without proper precautions, a discharge could occur between an astro-

naut on an extravehicular activity and a large space structure which would be fatal to the astronaut [2], [3]. Therefore, the ability to measure the charge on various objects from a distance will be important for missions involving rendezvous, docking, or proximity operations.

Though spacecraft charging has historically been viewed as a hazard to be mitigated, in recent years, many studies have investigated leveraging charged spacecraft to enable novel mission architectures. Missions are being proposed in which several smaller satellites flying in formation can accomplish tasks which would be difficult or impossible for a single, monolithic spacecraft (e.g., [4]). The Coulomb forces between multiple charged spacecraft can be used to create formations and virtual structures which require no traditional propellant [5]–[8]. Another concept involves using electrostatic forces to inflate membrane structures [9], [10]. As valuable orbital regions become increasingly congested with retired satellites and hazardous debris, the need for active debris removal has been firmly established [11], [12]. The Electrostatic Tractor is an elegant method which uses electrostatic forces to raise the orbits of debris at GEO to a graveyard orbit or detumble uncooperative objects without making physical contact [13], [14]. Additionally, satellite operators are looking to maximize the use of assets in orbit and orbital servicing concepts have been proposed for refueling, repair, or replacement of components. Such missions may enable satellite lifetimes to be extended or new satellites to be assembled from salvaged components [15]–[17]. These concepts, which are significant areas of research for future space operations, require close proximity operations, rendezvous and docking, knowledge of a nearby object’s characteristics, and/or physical contact. Remote potential sensing systems can fill a key gap in current knowledge of spacecraft charging, allowing for a better understanding of the negative impacts of undesired charging and significantly advancing the possible uses for electrostatics in space. This method can also provide scientific insight into how material properties change over time as materials degrade in the space environment because the charge state of an object depends on that object’s material properties.

C. Previous Work

Though spacecraft charging has been studied extensively, little work has been done on the topic of remote sensing of charge. Ferguson et. al propose in Reference [18] the concept of remote sensing of charging or arcing and consider various techniques to remotely monitor high-level charging or arcing events on satellites, including surface glows, bremsstrahlung x-rays, and radio or optical emission from arcing.

Bennett [19] discusses how the charge on one satellite in a two-craft formation can be estimated from the relative motion dynamics which are driven by the Coulomb force using range and range rate measurements. However, this method can provide only a single charge measurement for the entire target (i.e., an effective sphere model) and updates the charge estimate on the order of minutes. Therefore, a method with higher spatial and temporal resolution is desired. Engwerda [20], [21] proposes a method for sensing charge by directly measuring

the electric field around an object. This work focuses on how to use the voltage measurements to obtain a charge estimate and then develop a multi-sphere electrostatic model of the target [22]. However, the challenges of obtaining a direct electric field measurement near a charged object in plasma are not considered. Further, this preliminary work considers only planar circumnavigation with perfectly known relative motion.

Halekas et al. use secondary electrons and photoelectrons measured by the Lunar Prospector spacecraft to remotely map the charge distribution on the surface of the Moon [23], [24]. The measurements were completely passive, with the low energy electrons being generated by solar photons or plasma currents. Additionally, the authors compare the incident currents with the secondary currents to estimate the secondary electron yield of lunar regolith [25]. This reference demonstrates the feasibility of remotely mapping the charge and characterizing the material properties of a surface using electrons.

This paper presents prospects and challenges for using secondary electrons to remotely sense the potential of a closely neighboring space object. The paper is outlined as follows. Section II provides the theory of secondary and photo emission, and also discusses challenges of remote potential sensing. In Section III, computer simulations are used to investigate the trajectories of electrons in the vicinity of charged spacecraft. The effects of various geometries, relative distances, and potentials on the charge sensing method are considered. Two case studies are presented in Sections IV and V to demonstrate the feasibility of the concept.

II. THEORY AND CONCEPT

A. Secondary Electron Emission

When an energetic electron impacts a surface, it can interact with the surface in several ways. When an incident electron collides with an atomic electron and reflects back out of the material, it is called a backscattered electron. When an incident electron knocks an electron out of the atom which then escapes the surface, the emitted particle is called a secondary electron. Figure 2(a) shows a schematic of how secondary electrons are generated by an energetic particle impacting the surface. Figure 2(b) shows an example secondary electron yield curve. The secondary electron coefficient or yield, δ , is the probability that a secondary electron will be emitted for every primary electron that strikes the surface. This coefficient is a function of the primary electron energy and is different for every material. For many materials, the secondary electron coefficient exceeds unity for a given energy range. This implies that for every primary electron, multiple secondary electrons are emitted. Backscattered and secondary electrons can be differentiated because secondaries have energies less than 50 eV whereas backscattered electrons have energies greater than 50 eV [26]. Secondary electron energy distributions show that most secondaries are emitted with energies between 5 and 10 eV [27]. Secondary electrons are emitted from a surface with a cosine angular distribution about the surface normal that is independent of the angle of incidence of the primary electron [27]. The secondary yield, however, increases

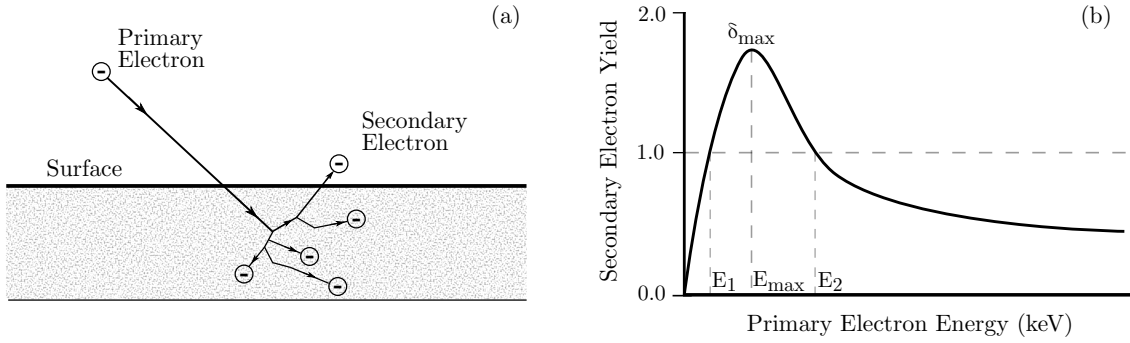


Fig. 2. (a) Depiction of secondary electron generation. (b) Example secondary electron yield curve.

with increasing incidence angle because more energy from the primary electron is deposited near the surface where secondaries have a high probability of escape.

B. Photoelectron Emission

Energy from the sun can energize electrons in the first few nanometers of the spacecraft so that they leave the surface. The current is given by [28]:

$$I_p = \begin{cases} j_{ph} A e^{-q\phi/k_B T_{ph}} & \phi > 0 \\ j_{ph} A & \phi \leq 0 \end{cases} \quad (1)$$

where j_{ph} is the photoelectron flux, A is the sunlit area, and $k_B T_{ph}$ is the thermal energy of the ejected photoelectrons. For aluminum, $k_B T_{ph} = 2$ eV and $j_{ph} = 40 \mu A/m^2$. For a negative spacecraft this current is constant, and for a positive spacecraft it quickly vanishes. Because most of the photoelectrons will be recaptured by a positive spacecraft, it will be very hard to measure positive potentials without the sensing craft being very positive.

C. Remote Sensing Using Electrons

The proposed method for remote potential sensing is enabled by the fact that secondaries and photoelectrons are emitted with very low energy. Therefore, the electron energy measured at the servicing craft is equivalent to the potential difference between the two craft.

Spacecraft surface charging is frequently discussed in the context of geosynchronous orbit (GEO) or deep space. In dense plasmas such as those in Low Earth Orbit, the ambient plasma density is sufficiently large that there will be thermal collisions between the secondary or photoelectrons. Similarly, the electric field between the two craft will be shielded out over short distances. Thus, the proposed technology is better suited to tenuous plasmas such as are found at GEO and beyond.

There are several challenges associated with using electrons for remote sensing. The first challenge is to ensure that a sufficient signal is obtained from the secondary or photo electron current such that it is observable by an instrument relative to the ambient plasma population. The electric field about a charged object falls off with the distance squared, so beyond some distance, the electrons of interest will be affected

by environmental fields and will no longer be distinguishable from background fluxes. This imposes requirements that the sensing craft be able to fly in proximity to the target object. Depending on the method of sensing and relative geometry, the sensing craft may need to operate within several craft radii of the target object. This is not problematic, however, as servicing, salvaging, docking, and remote actuation missions already propose flying in close proximity. Future studies will investigate the maximum distance at which the charge on an object can be sensed under various environmental conditions.

A similar challenge arises related to obtaining a sufficient number of electrons to measure. For forced charging applications such as the electrostatic tractor, an active electron beam is directed at the target which generally dominates the other currents to and from the object. Therefore, a large number of secondaries are generated which can be measured. For natural charging applications, the photoelectric current often dominates and therefore produces a large number of electrons which can be measured. However, if an electron beam is not used, the servicing craft must achieve a relative orbit such that it can observe the escaping photoelectrons. In other words, it must be on the sunlit side of the target object, which further imposes requirements on the mission. If the photoelectric current is not present at all (for example, in eclipse), it may be possible to use a short pulse from an electron beam to generate secondary electrons. A concern is how to generate secondaries without changing the charge state of the target which the servicing craft is attempting to measure. Future studies will investigate this and also whether secondaries generated by ambient plasma fluxes could be used for passive sensing of electrostatic potential.

Another challenge arises from the fact that spacecraft are composed of various components which may float at different potentials. Therefore, the electric field geometry about the spacecraft may be complex, with potentials wells and barriers which make it difficult to measure the emitted secondary electrons. Additionally, the sensing system may measure different peaks in the electron energy distribution associated with the differentially charged components. A sufficient spatial resolution of the sensing system is required to resolve the potentials of each component. As each material has unique secondary emission properties, there is a possibility for multiple electron populations from spacecraft components with different materi-

als and charge states. Finally, dielectrics and insulators, which are common on spacecraft surfaces, have different charging and secondary emission physics that conductors. Future work will investigate how the remote sensing technique can be implemented for realistic spacecraft materials and geometries.

The primary question to be investigated in the remainder of this paper is under what conditions is a sufficient number of secondary electrons captured to measure the charge of the target object. The following section describes the development and results of numerical studies used to investigate this question.

III. SIMULATION AND RESULTS

A. Simulation Setup

A 2-dimensional simulation was written in Matlab to analyze the feasibility for using low-energy electrons to remotely sense the charge of an object in space. Initially, each spacecraft was modeled as a single sphere so that the electric field can be computed straightforwardly. Voltages are assigned to the servicing craft and target object and then the charges are computed using the capacitance matrix [22], [29], [30] as:

$$\begin{bmatrix} q_S \\ q_T \end{bmatrix} = [C(\rho)] \begin{bmatrix} \phi_S \\ \phi_T \end{bmatrix} \quad (2)$$

$$[C(\rho)] = \frac{\rho}{k_c(\rho^2 - R_S R_T)} \begin{bmatrix} R_S \rho & -R_S R_T \\ -R_S R_T & R_T \rho \end{bmatrix}, \quad (3)$$

where $[C(\rho)]$ is the 2×2 capacitance matrix, ϕ_S and ϕ_T are the servicing craft and target object voltages respectively, q_S and q_T are the charges, R_S and R_T are the object radii, ρ is the center-to-center separation distance, and k_c is the Coulomb constant.

The total electric field at a given point is found by the following equation:

$$\mathbf{E} = k_c \frac{q_S \mathbf{r}_S}{r_S^3} + k_c \frac{q_T \mathbf{r}_T}{r_T^3}, \quad (4)$$

where \mathbf{r}_S and \mathbf{r}_T are the distances from the given point to the center of the servicing craft and target object, respectively. The force on each electron is computed at each timestep using the combined electrostatic and Lorentz force:

$$\mathbf{F} = q(\mathbf{E} + \mathbf{v} \times \mathbf{B}), \quad (5)$$

where q is the electron charge, \mathbf{v} is the velocity of each particle relative to the magnetic field which co-rotates with earth, and \mathbf{B} is the magnetic field. For these simulations, a magnetic field strength of 100 nT directed out of the simulation plane was selected to represent the field at GEO, though the effect is very small. Mutual repulsion between electrons and effects of beam-expansion into a vacuum are neglected. The spacecraft are assumed to be perfectly geostationary so the velocity of the electrons with respect to the spacecraft is also the velocity with respect to the B field. A user-specified number of electrons are generated with initial energies of 5 eV at the surface of the target and an initial velocity distribution consistent with the cosine distribution relative to the local surface normal. At each timestep, the electric field is computed at each particle, then the forces are used to compute the next state using a fourth-order Runge-Kutta method with a variable timestep. Individual

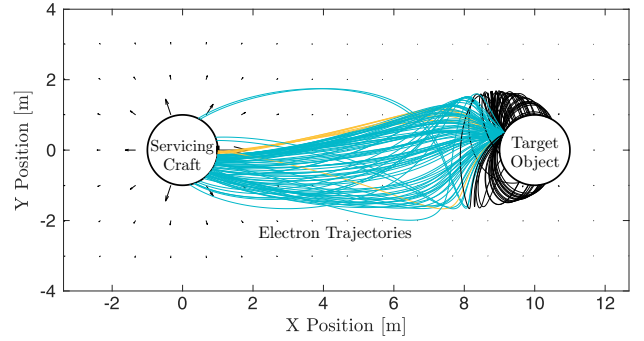


Fig. 3. Simulation results for an application with low charging levels and passive sensing. The electrons with black trajectories do not escape the target object's potential well, those with blue trajectories impact the servicing craft, and those with gold trajectories enter a 25 cm² detector on the front of the servicing craft. The black arrows denote the direction and relative magnitude of the electric field.

electrons which impact either craft or leave the simulation domain are stopped. At the conclusion of the simulation, the electrons which hit either the servicing craft or a designated sensor on the servicing craft are counted. This allows the fraction of detected particles to be computed and thus provides insight into the expected signal-to-noise ratio, as is discussed later on.

Figure 3 shows an example of the simulation results for a case where a 1 m radius target object is charged to +20 V, the 1 m radius servicing craft to +100 V, and the two craft are separated by 10 m. The particles are generated 0.5 m above the X-axis on the target object. Because the target is slightly positive, some of the secondary electrons (black trajectories) do not have the energy to escape the potential well and thus return to the target. Other electrons escape the target object and impact the servicing craft (blue trajectories), and a small number (gold trajectories) enter a 25 cm² sensor on the front of the servicing craft. As a numerical check, the particles captured by the servicing craft are confirmed to have energies between 80 and 85 eV (depending on the initial energy). This simulation demonstrates that even if the target object is charged positively, the servicing craft can measure the energy of the secondary electron population, as long as it is more positive than the target.

Figure 4 shows results for a case simulating operation of the Electrostatic Tractor so that both craft achieve potentials with very large magnitudes. In this simulation, the servicing craft is charged to +20 kV, the target object is charged to -20 kV, and electrons are generated on the target between 0 and 20 cm above the Y-axis. Again, the simulation confirms that the electrons arrive at the servicing craft with energies of approximately 40 keV. For applications with such high charging levels, there is a much smaller region on the target for which electrons will map onto the sensing detector.

B. Parameter Trade Studies

An important quantity for determining the feasibility of the proposed method is the fraction, α , of the emitted secondary electron current, I_{SEE} , which is captured by the detector on the servicing craft, I_{SEC} . This fraction is a function of the object

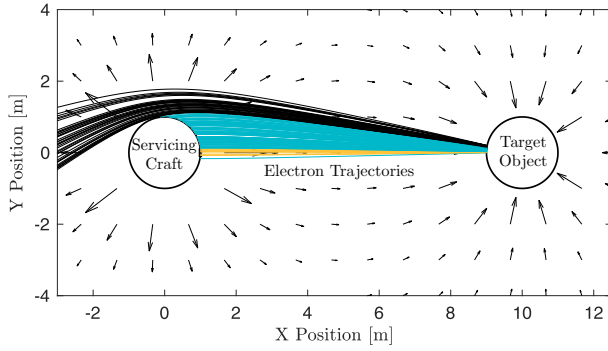


Fig. 4. Simulation results for an application with high, forced charging levels and active sensing. The electrons with black trajectories escape into space, those with blue trajectories impact the servicing craft, and those with gold trajectories enter a 25 cm² detector on the front of the servicing craft. Again, the black arrows denote the direction and relative magnitude of the electric field.

potentials, the separation distance, and the relative geometry between the two craft. A broad range of simulations have been run to investigate this parameter space and determine the conditions for which the secondary electron method for remote potential sensing may be feasible. Figure 5 shows the fraction α plotted as a function of the servicing craft voltage, V_S , and the separation distance, L . In this simulation, the target object voltage, V_T , is held fixed at -100 V. Both craft are assumed to be spheres of radius 1 m, the detector on the servicing craft is defined to be 25 cm², and the secondaries are generated along a 40 cm² area on the target object surface centered about the line of separation. The results show that the captured current depends most significantly on the separation distance. For separation distances of a few craft radii, the captures current is tens of percent of the emitted current. Beyond 10 meters separation, the captured current decreases from 10 to a few percent of the emitted current. For forced charging applications where I_{SEE} is large, the remote potential sensing method would be feasible at operating distances of 10s of meters. For other applications where I_{SEE} is small, it may be necessary to operate at separations of a few craft radii to obtain a sufficient signal to noise ratio. Sections IV and V provide case studies for specific operating conditions within each regime.

Figure 6 shows how α depends on the voltage of both the servicing and target craft. The separation distance is fixed at 10 m and the same assumptions regarding the initial condition of the secondaries and the detector size are made again here. The highest value of α occurs when V_T is at the lowest magnitude potential and V_S is at the highest. This occurs because the electrons are not strongly accelerated away from the target at which they are generated, but are strongly accelerated toward the servicing craft. Therefore, the servicing craft collects a large fraction of the secondaries. Conversely, when V_T is large negative and V_S is small positive, α is very small. In this case, the electrons gain most of their energy when leaving the target surface and their trajectories are essentially determined before they are influenced by the servicing craft electric field. Therefore, only those electrons which are accelerated along the

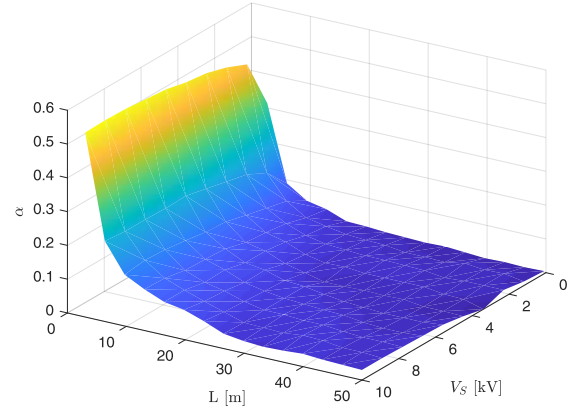


Fig. 5. Value of α as a function of separation distance and servicing craft voltage.

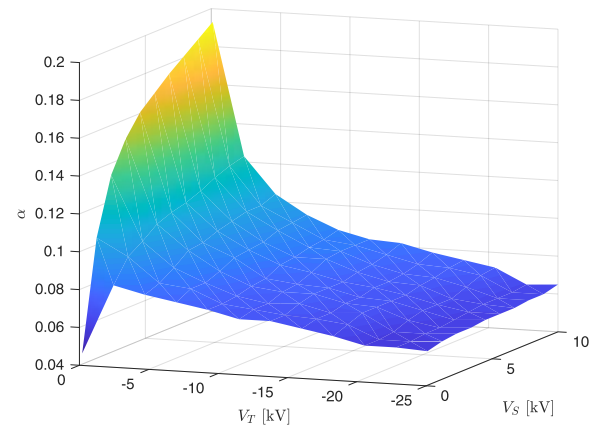


Fig. 6. Value of α as a function of the target object and servicing craft voltages.

line between the two craft will be captured by the detector. Interestingly, α is lowest where both V_T and V_S are small in magnitude. In this case, the electrons are not accelerated strongly and therefore travel slowly away from the target surface. Therefore, the initial velocities of the electrons are important and the initial cosine angular distribution has time to expand such that only a small percentage of the secondaries map onto the detector.

C. Rectangular Spacecraft Study

Another simulation was run to investigate the trajectories of electrons around charged spacecraft with more realistic and geometrically complex shapes. The Method Of Moments (MOM) was used to find the electric field in the vicinity of the two spacecraft due to the voltage of both of them. The MOM is an elastance-based method which translates the voltage to charge on every node through an extension of Poisson's law [31]. Once the charge is found every node, the E field can be computed at an arbitrary point in space.

For this simulation, a 1 meter cube is charged to +20 kV and a 2 × 1 meter rectangular box charged to -20 kV is 15

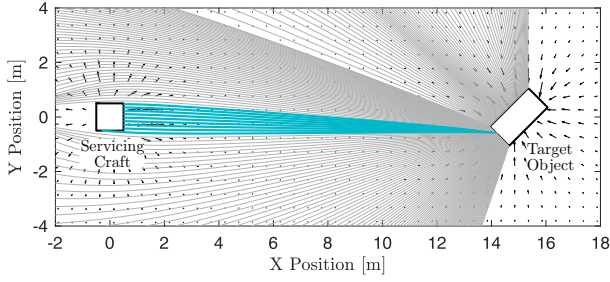


Fig. 7. Simulation results for two non-spherical spacecraft. The electrons with gray trajectories escape into space, those with blue trajectories impact the servicing craft.

meters away and rotated by 45° . 144 polygons are used per square meter and the E field is computed at 900 points in the XY-plane. This E field is then interpolated for trajectories that do not lie directly on the field points.

Figure 7 shows the results of this study. In this simulation, electrons are generated on every surface of the target which is visible to the servicing craft. When the target is charged to potentials in the kV range, the electrons will quickly reach high velocities as they fly away from the surface. Therefore, their trajectories are mostly determined by the field geometry at the target object and are not influenced significantly by the servicing craft. As shown in the figure, there is a small region on the target from which the electric field points to the servicing craft and the electrons make it to the craft (these trajectories are colored blue). By expanding the electron beam size such that it illuminates the entire target, it is possible to guarantee that some secondary electrons on the target will always map back to the servicing craft. Future research will investigate sensing performance given more complex spacecraft geometries and the effects of a tumbling target.

IV. CASE STUDY FOR ELECTROSTATIC TRACTOR

To demonstrate feasibility of remote potential sensing, a case study was carried out with application to the Electrostatic Tractor. Hogan and Schaub [32] provide an example operating condition for the Electrostatic Tractor: a tractor of 2 m radius is charged to 21.5 kV, a debris object of radius 0.935 m is charged to -15.3 kV with a separation distance of 12.5 m. The electron beam energy is E_{EB} 40 keV and the beam current is $I_{beam} = 520 \mu A$. Further, it is assumed that the beam diameter is 20 cm and the beam impacts the target sphere centered on the line of separation. The trajectories of 2000 particles are simulated with initial energies of 10 eV and a cosine angular distribution. The secondary electron emission current model is given by:

$$I_{SEE} = -4Y_M I_{beam} \kappa, \quad (6)$$

where

$$\kappa = \frac{E_{eff}/E_{max}}{(1 + E_{eff}/E_{max})^2}, \quad (7)$$

$E_{eff} = E_{EB} - q\phi_S + q\phi_T$. Y_M is the peak of the secondary electron yield curve and E_{max} is the energy at which this peak

occurs [33]. Values of $Y_M = 1$ and $E_{max} = 300$ eV are assumed, so $I_{SEE} = 163 \mu A$.

The secondary electron current captured by the detector on the servicing craft, I_{SEC} , is found by:

$$I_{SEC} = \alpha I_{SEE}, \quad (8)$$

where α is between 0 and 1. For these conditions, the numerical simulation results show that 15.3% of the secondary electrons are captured by the 25 cm^2 detector centered on the tractor satellite. Therefore $\alpha = 0.153$ and $I_{SEC} = 25.0 \mu A$.

The flux of secondary electrons occurs at a very narrow range of energies corresponding to the potential difference between the two craft plus the initial energy of the electrons. The captured secondary current is converted to a flux so that it can be compared to ambient electron fluxes. This flux, F_{SEC} , is modeled as a Gaussian function with a mean equal to the average final kinetic energy of the simulated electrons which are captured, $\mu = 36.24$ keV, and a standard deviation $\sigma = 50$ eV. Figure 8 shows the secondary electron flux superimposed on a bi-Maxwellian background. The bi-Maxwellian model parameters were selected to be representative of storm-time conditions in GEO, with $n_1 = 0.3 \text{ cm}^{-3}$, $T_1 = 4$ keV, $n_2 = 0.2 \text{ cm}^{-3}$, and $T_2 = 7$ keV [34].

$$F = \sum_{i=1}^2 n_i \sqrt{\frac{q}{2\pi T_i m_e}} \frac{q\phi_S}{k_B T_i} \exp\left(\frac{q\phi_S}{k_B T_i}\right) \quad (9)$$

where k_B is the Boltzmann constant and m_e is the electron mass. Figure 8 shows the electron flux at the sensing craft, including both the ambient plasma and the secondary electron population. The dashed black line shows the expected value of the secondary population energy, equal to $\phi_S - \phi_T = 36.8$ keV. The actual peak is slightly less than this due to numerical error from the fact that the spacecraft are modeled as point charges and modeled electric field is therefore slightly weaker than it would be with a higher fidelity field model. Figure 9 shows the count rates which would be observed by an electron energy analyzer on the servicing craft with an energy resolution of $\Delta E/E = 8\%$ and a geometric factor of $2 \times 10^{-5} \text{ cm}^2 \text{ sr keV}$. These values are consistent with plasma analyzers which have been used for on-orbit and laboratory experiments (e.g., [35]–[37]). A more detailed analysis of the instrument performance and requirements is left for future studies. The secondary electron peak is several orders of magnitude higher than the background. This is because the detected secondary electron current is already large and, further, the secondary electrons are limited to a very narrow energy range. Even for geometries in which the majority of the secondary electrons escape into space, the signal peak from a small percentage of captured electrons provides sufficient information for the potential of the target object to be determined. In light of these results, the proposed method for remote potential sensing is feasible for the Electrostatic Tractor application given current technologies.

V. CASE STUDY FOR PASSIVE SENSING APPLICATIONS

Another case study is presented to determine the feasibility of passive sensing of potential using photoelectrons. An operating condition is assumed in which the sensing craft and

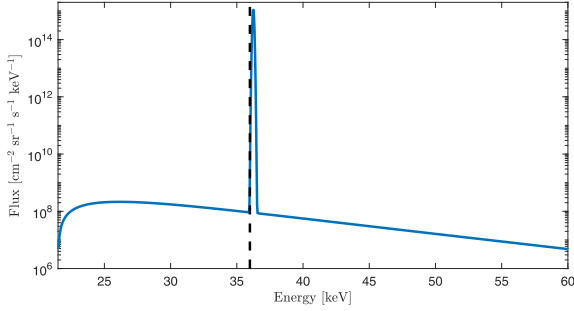


Fig. 8. Electron fluxes for the Electrostatic Tractor remote potential sensing case study. The background fluxes are a bi-Maxwellian and the peak is the secondary electron signal. The dashed black line represents the expected energy value.

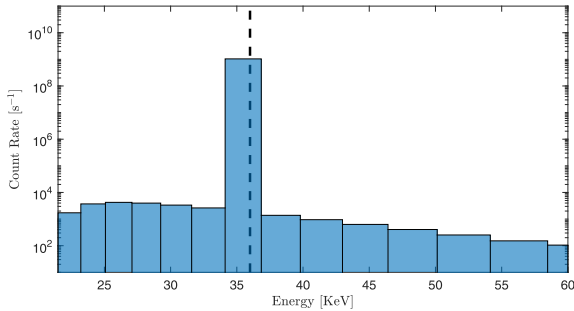


Fig. 9. Model of observed electrostatic analyzer signal for the Electrostatic Tractor remote potential sensing case study, in which the fluxes have been binned assuming an instrument resolution of 8%.

target object are spheres of 1 meter radius, separated by 8 m, with $\phi_S = 200$ V and $\phi_T = -50$ V. The target is assumed to be a conducting, aluminum sphere with $j_{ph} = 40 \mu\text{A}/\text{m}^2$ and $k_B T_{ph} = 2$ eV. It is assumed that the half of the target sphere facing the servicing craft is in sunlight. Under these conditions, only 1.75% of the emitted photoelectrons are captured by the sensor on the servicing craft. This percentage is small because photoelectrons are generated on a large area of the target craft, but only a small area maps back to the sensor. Assuming the sunlit area is a circle, the emitted photoelectron current is $126 \mu\text{A}$. Given $\alpha = 0.175$, the current captured by the servicing craft sensor is $2.2 \mu\text{A}$. As in the previous section, the photoelectron population is modeled as a Gaussian with a mean equal to the average final kinetic energy of the captured electrons, $\mu = 247$ eV, and a standard deviation of $\sigma = 1$ eV. The same bi-Maxwellian distribution used in the previous section is used again here. Figure 10 shows the photoelectron population flux superimposed on the bi-Maxwellian background. The dashed black line shows the expected energy. The peak photoelectron flux is several orders of magnitude larger than the background flux, therefore the signal is easily detectable given current energy analyzer capabilities. In light of this result, remote potential sensing is feasible for passive sensing applications in which only photoelectrons are used.

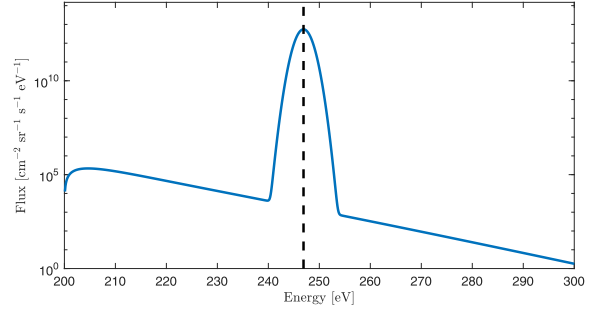


Fig. 10. Electron fluxes for the photoelectron remote potential sensing case study. The dashed black line represents the expected energy value of the photoelectrons. Note that units of eV are used instead of keV.

VI. CONCLUSION AND FUTURE WORK

This paper presents the prospects for how electrons can be used to remotely sense the charge on a space object, as well as the challenges for further development. Using either secondaries from an active electron beam or the photoelectron current, the potential on an object can be sensed over distances of tens of meters in geosynchronous orbit with realistic instrumentation. Several challenges are identified which will be addressed in future work. Realistic spacecraft geometries may produce potential wells and barriers that complicate the measurement. Similarly, sensing of charge for differentially charged spacecraft with material properties that are not well characterized similarly may not be straightforward. Future studies will incorporate more sophisticated electrostatic and secondary electron emission models to study such scenarios. Laboratory experiments both in vacuum and in plasma are planned to demonstrate the concept with a variety of materials, geometries, and charge regimes, and also validate the numerical results.

ACKNOWLEDGMENT

The authors would like to thank Jordan Maxwell, Kieran Wilson, Ryan Hoffman, and Zoltan Sternovsky for fruitful discussions on this topic.

REFERENCES

- [1] D. Barnhart, B. Sullivan, R. Hunter, J. Bruhn, E. Fowler, L. M. Hoag, S. Chappie, G. Henshaw, B. E. Kelm, T. Kennedy *et al.*, "Phoenix program status-2013," in *AIAA Space 2013 Conference and Exposition*, 2013, p. 5341.
- [2] M. Carruth, Jr, T. Schneider, M. McCollum, M. Finckenor, R. Suggs, D. Ferguson, I. Katz, R. Mikatarian, J. Alred, and C. Pankop, "Iss and space environment interactions without operating plasma contactor," in *39th Aerospace Sciences Meeting and Exhibit*, 2001, p. 401.
- [3] D. Ferguson, T. Morton, and G. Hillard, "First results from the floating potential probe (fpp) on the international space station," in *39th Aerospace Sciences Meeting and Exhibit*, 2001, p. 402.
- [4] M. Martin and M. Stallard, "Distributed satellite missions and technologies-the techsat 21 program," in *Space Technology Conference and Exposition*, 1999, p. 4479.
- [5] L. B. King, G. G. Parker, S. Deshmukh, and J.-H. Chong, "Spacecraft formation-flying using inter-vehicle coulomb forces," NASA/NIAC, Tech. Rep., January 2002.
- [6] H. Schaub and L. E. Z. Jasper, "Orbit boosting maneuvers for two-craft coulomb formations," *AIAA Journal of Guidance, Control, and Dynamics*, vol. 36, no. 1, pp. 74–82, Jan. – Feb. 2013.

- [7] H. Joe, H. Schaub, and G. G. Parker, "Formation dynamics of coulomb satellites," in *6th International Conference on Dynamics and Control of Systems and Structures in Space*, Riomaggiore, Cinque Terre, Italy, July 2004, pp. 79–90.
- [8] H. Schaub, G. G. Parker, and L. B. King, "Challenges and prospect of coulomb spacecraft formation control," *Journal of the Astronautical Sciences*, vol. 52, no. 1–2, pp. 169–193, Jan.–June 2004.
- [9] L. A. Stiles, H. Schaub, K. K. Maute, and D. F. Moorer, "Electrostatically inflated gossamer space structure voltage requirements due to orbital perturbations," *Acta Astronautica*, vol. 84, pp. 109–121, Mar.–Apr. 2013. [Online]. Available: <http://www.sciencedirect.com/science/article/pii/S0094576512004584>
- [10] L. A. Stiles, H. Schaub, K. Maute, and D. F. Moorer, "Electrostatic inflation of membrane space structures," in *AAS/AIAA Astrodynamics Specialist Conference*, Toronto, Canada, Aug. 2–5 2010, aIAA-2010-8134.
- [11] P. V. Anderson and H. Schaub, "Local debris congestion in the geosynchronous environment with population augmentation," *Acta Astronautica*, vol. 94, no. 2, pp. 619–628, Feb., 2014.
- [12] H. Schaub, L. E. Z. Jasper, P. Anderson, and D. S. McKnight, "Cost and risk assessment for spacecraft operation decisions caused by the space debris environment," *Acta Astronautica*, vol. 113, pp. 66–79, August–September 2015.
- [13] H. Schaub and D. F. Moorer, "Geosynchronous large debris reorbiter: Challenges and prospects," *The Journal of the Astronautical Sciences*, vol. 59, no. 1–2, pp. 161–176, 2012.
- [14] T. Bennett, D. Stevenson, E. Hogan, L. McManus, and H. Schaub, "Prospects and challenges of touchless electrostatic detumbling of small bodies," *Advances in Space Research*, vol. 56, no. 3, pp. 557–568, 2015.
- [15] D. A. Whelan, E. A. Adler, S. B. Wilson, and G. M. Roesler, "Darpa orbital express program: effecting a revolution in space-based systems," in *Small Payloads in Space*, vol. 4136. International Society for Optics and Photonics, 2000, pp. 48–57.
- [16] A. Ellery, J. Kreisel, and B. Sommer, "The case for robotic on-orbit servicing of spacecraft: Spacecraft reliability is a myth," *Acta Astronautica*, vol. 63, no. 5–6, pp. 632–648, 2008.
- [17] B. Sullivan, D. Barnhart, L. Hill, P. Oppenheimer, B. L. Benedict, G. Van Ommering, L. Chappell, J. Ratti, and P. Will, "Darpa phoenix payload orbital delivery system (pods):fedex to geo," in *AIAA SPACE 2013 conference and exposition*, 2013, p. 5484.
- [18] D. C. Ferguson, J. Murray-Krezan, D. A. Barton, J. Dennison, and S. A. Gregory, "Feasibility of detecting spacecraft charging and arcing by remote sensing," *Journal of Spacecraft and Rockets*, vol. 51, no. 6, pp. 1907–1913, 2014.
- [19] T. J. Bennett, "On-orbit 3-dimensional electrostatic detumble for generic spacecraft geometries," Ph.D. dissertation, University of Colorado Boulder, 2017.
- [20] H. Engwerda, J. Hughes, and H. Schaub, "Remote sensing for planar electrostatic characterization using the multi-sphere method," in *Final Stardust Conference, ESTEC, The Netherlands*, Oct 2016.
- [21] H. Engwerda, "Remote sensing for spatial electrostatic characterization using the multi-sphere method," Master's thesis, Delft University of Technology, Delft, The Netherlands, March 2017.
- [22] D. Stevenson and H. Schaub, "Multi-sphere method for modeling electrostatic forces and torques," *Advances in Space Research*, vol. 51, no. 1, pp. 10–20, Jan. 2013.
- [23] J. Halekas, D. Mitchell, R. Lin, L. Hood, M. Acuña, and A. Binder, "Evidence for negative charging of the lunar surface in shadow," *Geophysical research letters*, vol. 29, no. 10, 2002.
- [24] J. Halekas, G. Delory, R. Lin, T. Stubbs, and W. Farrell, "Lunar prospector observations of the electrostatic potential of the lunar surface and its response to incident currents," *Journal of Geophysical Research: Space Physics*, vol. 113, no. A9, 2008.
- [25] —, "Lunar prospector measurements of secondary electron emission from lunar regolith," *Planetary and Space Science*, vol. 57, no. 1, pp. 78–82, 2009.
- [26] T. Kaneko, "Energy distribution of secondary electrons emitted from solid surfaces under electron bombardment: I. theory," *Surface Science*, vol. 237, no. 1–3, pp. 327–336, 1990.
- [27] H. Bruining, *Physics and Applications of Secondary Electron Emission: Pergamon Science Series: Electronics and Waves Series of Monographs*. Elsevier, 1954.
- [28] S. T. Lai, *Fundamentals of Spacecraft Charging: Spacecraft Interactions with Space Plasmas*. Princeton University Press, 2011.
- [29] C. R. Seubert, L. A. Stiles, and H. Schaub, "Effective coulomb force modeling for spacecraft in earth orbit plasmas," *Advances in Space Research*, 2014.
- [30] W. R. Smythe, *Static and Dynamic Electricity*, 3rd ed. McGraw–Hill, 1968.
- [31] W. C. Gibson, *The method of moments in electromagnetics*. Chapman & Hall, November 28 2007.
- [32] E. Hogan and H. Schaub, "Space weather influence on relative motion control using the touchless electrostatic tractor," *Journal of Astronautical Sciences*, vol. 63, no. 3, pp. 237–262, 2016.
- [33] B. T. Draine and E. E. Salpeter, "On the physics of dust grains in hot gas," *Astrophysical Journal*, vol. 231, pp. 77–94, July 1979.
- [34] V. Davis, B. Gardner, M. Mandell, and K. Wilcox, *NASCAP-2k User's Manual*, 4th ed., Science Applications International Corporation, San Diego, CA 92121, February 2011.
- [35] H. Funsten, R. Skoug, A. Guthrie, E. MacDonald, J. Balonado, R. Harper, C. Henderson, K. Kihara, J. Lake, B. Larsen *et al.*, "Helium, oxygen, proton, and electron (hope) mass spectrometer for the radiation belt storm probes mission," *Space Science Reviews*, vol. 179, no. 1–4, pp. 423–484, 2013.
- [36] A. L. Victor, T. H. Zurbuchen, and A. D. Gallimore, "Top hat electrostatic analyzer for far-field electric propulsion plume diagnostics," *Review of scientific instruments*, vol. 77, no. 1, p. 013505, 2006.
- [37] J. McFadden, C. Carlson, D. Larson, M. Ludlam, R. Abiad, B. Elliott, P. Turin, M. Marckwordt, and V. Angelopoulos, "The themis esa plasma instrument and in-flight calibration," *Space Science Reviews*, vol. 141, no. 1–4, pp. 277–302, 2008.